Electron Transport through Cyclic Disulfide Molecular Junctions with Two Different Adsorption States at the Contact: A Density Functional Theory Study

ARTICLE *in* THE JOURNAL OF PHYSICAL CHEMISTRY C · MAY 2008

Impact Factor: 4.77 · DOI: 10.1021/jp800201z

2 AUTHORS, INCLUDING:

William A. Goddard
California Institute of Technology
1,337 PUBLICATIONS **68,337** CITATIONS

SEE PROFILE

Electron Transport through Cyclic Disulfide Molecular Junctions with Two Different Adsorption States at the Contact: A Density Functional Theory Study

Yun Hee Jang[‡] and William A. Goddard III*,[†]

Materials and Process Simulation Center (139-74), California Institute of Technology, Pasadena, California 91125, Department of Materials Science and Engineering, Gwangju Institute of Science and Technology, Gwangju 500-712, Korea, and LEMA, Université François Rabelais, 37200 Tours, France

Received: January 9, 2008

1,2-Dithiolane is a promising anchor group for attaching molecules to metal electrodes in molecular junction devices. This five-membered cyclic disulfide adsorbs on Au surfaces either in a *cyclic* fashion (with its disulfide bond *intact*, via molecular adsorption) or in an *acyclic* fashion (with its disulfide bond *broken*, via dissociative adsorption). Our density functional theory calculations show that the dissociative adsorption is slightly preferred, but both are stable. We also report nonequilibrium Green's function calculations showing that molecular junctions of cyclic and acyclic 1,2-dithiolanes sandwiched between two gold electrodes exhibit essentially the same insulating current–voltage characteristics at moderate bias voltages, despite the significant difference in their states of adsorption.

1. Introduction

Molecular electronics involves bottom-up manufacturing of electronic devices composed of single-molecule or self-assembled monolayer (SAM) junctions.[1,2] One of the essential components of molecular junction devices is the anchor group that attaches each molecule to the electrode. Understanding the behavior of the anchor group is crucial for the development of robust molecular junctions.

Cyclic disulfides such as 1,2-dithiolane [$S(CH_2)_3S$] have recently attracted considerable attention as "alligator clips" to metal (especially gold) surfaces to make robust SAMs.[3] Compounds such as 1,2-dithiolane-3-pentanoic acid (also known as thioctic acid, lipoic acid, or 1,2-dithiolane-3-valeric acid) have been used for various applications such as molecular switches, molecular machines, sensors, and protein immobilization.[4–14] A prominent example is the bistable Stoddart−Heath-type [2]rotaxane (**1**) anchored to gold electrodes,[4,15] which has already proved useful as a molecular switch.[15,16]

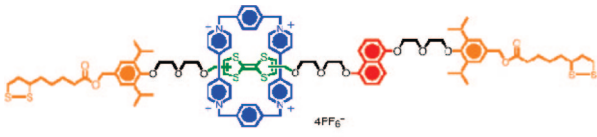

1

The switch **1** is turned on and off reversibly upon the redox-induced shuttling of the cyclobis-(paraquat-*p*-phenylene) (CBPQT, blue) ring between two stations, tetrathiafulvalene (TTF, green) and 1,5-dioxynaphthalene (DNP, red). Concrete evidence for the shuttle motion in solution has been provided by its X-ray crystal structure and its spectroscopic and electrochemical behavior,[17,18] as well as by first-principles quantum mechanics (QM) calculations.[19] In addition, QM calculations[20–22] showed that the resting state with the CBPQT ring on the TTF unit is off (low current) and the state with the ring on the DNP unit is on (high current). This change in conductance arises because the on state has nearly degenerate HOMOs (and LUMO) on the two units, whereas the off state has very different energy levels. However, not much is known about the behavior of **1** on electrode surfaces. Theoretical studies on the structure of the rotaxane-based SAM on a gold surface[23–25] found a large conductivity change upon shuttling.[26] However, the activation barrier to shuttling is high in solution (15−17 kcal/mol)[27–29] and even higher in a polymer matrix or in a SAM environment (18−20 kcal/mol).[27,30] Robust molecular junctions seem to have tightly packed SAMs,[23,24,31] which would not be a favorable environment for shuttling. Consequently, we have considered whether there might be a switching mechanism other than shuttling.

We note that molecular junctions employing **1** operate under a wide range of bias voltages up to ±2 V or under redox conditions to push the shuttle out of each station by oxidation–reduction. These conditions might also lead to redox processes involving disulfide and Au−S bonds.[32–35] Indeed, the irreversible oxidation peak at 0.90 V observed for alkanetetrathiols is attributed to oxidation of thiol groups, leading to the formation of disulfide linkages.[36] It was also reported that dissociation of dimethyl disulfide (CH_3SSCH_3) adsorbed on the Au(111) surface can be accomplished by applying a voltage of ∼1.4 V.[37] Existence of disulfide bonds has long been a controversy for alkanethiols and dialkyl disulfides adsorbed on gold surfaces.[37–45]

Thus, we posed the following questions: What if the application of the bias voltage induces the formation or breakage of the disulfide bonds of **1**? Would this conversion between *cyclic* and *acyclic* 1,2-dithiolane anchor groups alter the electron transport through **1**, serving as an additional switching mechanism for **1** and affecting the robustness of the junction?

To test this idea, we carried out QM calculations on a model of 1,2-dithiolane molecular junctions to establish (1) whether the disulfide bond of 1,2-dithiolane is *intact* or *broken* on

* To whom correspondence should be addressed. Phone: 626-395-2731. Fax: 626-585-0918. E-mail: wag@wag.caltech.edu.
† California Institute of Technology.
‡ Gwangju Institute of Science and Technology and Université François Rabelais.

10.1021/jp800201z CCC: $40.75
Published on Web 05/14/2008

SCHEME 1: Adsorption of 1,2-Dithiolane: Cyclic or Acyclic?

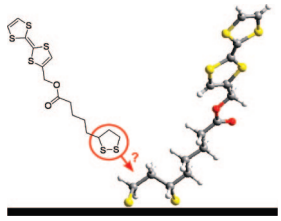

Au(111) surface and (2) how the presence of this bond affects the current–voltage ($I-V$) characteristics of the junction.

We calculated the most stable adsorption structures and the binding energies for both forms of 1,2-dithiolane (see Scheme 1), cyclic (with the S—S bond intact) and acyclic (with the S—S bond broken), on both the Au(111) surface and a Au_{28} cluster. Next, we used these most stable adsorption structures for each form to build a model junction of 1,2-dithiolane and then calculated the $I-V$ curve. We interpreted the results in terms of the electronic structure using the density of states (DOS) and projected DOS (PDOS) representations.

2. Calculation Methods

2.1. 1,2-Dithiolane/Au_{28}. The density functional theory (DFT) QM calculations on finite clusters (Au_{28}) were carried out using Jaguar v5.5 software.[46] The three-layer 28-atom cluster Au_{28}(9,10,9) (as shown below in Figure 3, section 3.2) has been established to be the minimum cluster size required for an accurate representation of the (111) surface of the fcc metal.[47] It was cut from a bulk Au crystal with an experimental lattice parameter of 4.08 Å, which corresponds to the nearest-neighbor Au—Au distance of 2.88 Å.[48] The Au atoms were kept fixed at their bulk positions throughout the geometry optimization of clean and adsorbed clusters.

For these calculations, we used the B3LYP[49–53] and PBE[54,55] functionals of DFT. The Au atoms were described using the Hay—Wadt small-core effective core potential (LACVP), with the outermost 19 electrons treated explicitly using the LACVP** basis set.[56,57] For the other atoms, all electrons were treated explicitly with the 6-31G** basis set. The triplet states were calculated using spin-unrestricted DFT, whereas the singlet states were calculated with spin-restricted DFT.

2.2. 1,2-Dithiolane/Au(111). QM calculations on periodic Au(111) slabs were carried out using an LCAO (linear combination of atomic orbitals) type of DFT as implemented in the SeqQuest code.[58–60] We used the PBE functional of DFT.[54,55] The core electrons of each atom were replaced by norm-conserving pseudopotentials,[61–64] and the outer electrons were described by a double-ζ-plus-polarization (DZP) basis set.[65] A smaller single-ζ-plus-polarization (SZP) basis set was also used for Au. The pseudopotentials and basis sets for Au were taken as optimized and tested in closely related previous calculations.[22,66,67] The DZP and SZP basis sets used for Au are listed in the Supporting Information.

These pseudopotentials and basis sets lead to an optimum lattice constant of 4.16 Å for the bulk Au crystal, which is only 2% larger than the experimental value. To avoid ambiguities in comparing cluster and slab calculations, we used the experimental lattice constant of 4.08 Å for both. We modeled the Au(111) surface using a rectangular ($3\sqrt{3} \times 5$) unit cell (30 Au atoms per layer) of a three-layer Au(111) slab (Au_{90}) (as shown below in Figure 4, section 3.2) with cell parameters of 14.99 × 14.42 × 23.56 (in Å). We used 94 × 90 × 150 points for the real-space grid (~0.16 Å/grid) and only the Γ point for the Brillouin zone sampling. All Au atoms were kept fixed at their bulk positions throughout the geometry optimization of clean and adsorbed slabs. (The Au atoms in the top layer were relaxed in another set of calculations for comparison.)

2.3. $I-V$ Calculations. The $I-V$ curves for the model devices with an electrode—SAM—electrode configuration (as shown below in Figure 5, section 3.3) were calculated using the Landauer—Büttiker formalism and nonequilibrium Green's function (NEGF) approach coupled with the LCAO type of DFT as implemented in SeqQuest.[59,67,68] See ref 67 for details of the method. It should be noted that we employed a non-self-consistent NEGF approach, which is valid only in the low-bias regime.[67]

The SAM on the bottom electrode was built by positioning the optimized 1,2-dithiolane in a (3 × 2) unit cell of a three-layer Au(111) slab. Each unit cell had six surface Au atoms and could accommodate two sulfur atoms of 1,2-dithiolane at the typical coverage of an alkanethiol SAM on Au(111) ($\theta = {}^1/_3$). This corresponds to a footprint of 0.432 nm^2 per 1,2-dithiolane molecule, which is close to those observed for the saturation coverage of thioctic acid SAMs (0.47 and 0.54 nm^2).[10,13] The SAM on the bottom electrode was replicated in a symmetrical fashion to build a SAM on the top electrode, which was again modeled by a three-layer Au(111) slab. Then, the two slabs were connected to each other via the $-CH_2CH_2-$ alkyl chain at the β-carbon (C4) position. The unit cell was repeated periodically in the a, b, and c directions so that the two Au(111) slabs (infinite in the a and b directions) in the top and bottom electrodes were stacked (in c direction) on each other smoothly as in the bulk. The dimensions of the final unit cell were 8.65 × 5.77 × 23.57 (in Å) with $\beta = 120°$ for both devices.

The DFT calculations used 54 × 36 × 148 points for the real-space grid (~0.16 Å/grid) and 2 × 3 × 1 k points for the Brillouin zone. The PBE functional of DFT was used with the DZP basis sets for C, H, and S. Because the calculations employing the DZP and SZP basis sets for Au predicted similar binding preferences of 1,2-dithiolane on Au(111) (within 2 kcal/mol; see Table 2 of section 3.3), we used the smaller SZP basis set for Au in the $I-V$ curve calculations.

3. Results and Discussion

3.1. 1,2-Dithiolane in the Gas Phase. The geometry of 1,2-dithiolane with the intact disulfide bond (cyclic 1,2-dithiolane) was taken from the crystal structure of DL-6-thioctic acid[69] and optimized in the gas phase using B3LYP. The final structure had a S—S distance of 2.120 Å and a CSSC dihedral angle of 33.0°, in agreement with the crystal structurevalues (2.053 Å and 34.5°). Then, we dissociated the disulfide bond to make acyclic 1,2-dithiolane and optimized the structures for various conformers in the triplet state ($S = 1$).

Based on the energy change from the singlet cyclic 1,2-dithiolane to the best conformer of the acyclic triplet, we calculated the gas-phase dissociation energies of the disulfide bond in 1,2-dithiolane to be 46.7 (ΔE), 45.4 (ΔH at 298 K), and 44.3 (ΔG at 298 K) kcal/mol. With the PBE functional, these bond energies were found to be 50.9 (ΔE), 49.9 (ΔH at 298 K), and 47.1 (ΔG at 298 K) kcal/mol.

The two functionals of DFT result in quite different electronic structures for 1,2-dithiolane (Figure 1). The HOMO–LUMO gaps calculated with B3LYP (4.6 and 2.1 eV for cyclic and acyclic 1,2-dithiolane, respectively) are significantly larger than those calculated with PBE (3.1 and 0.4 eV), as observed

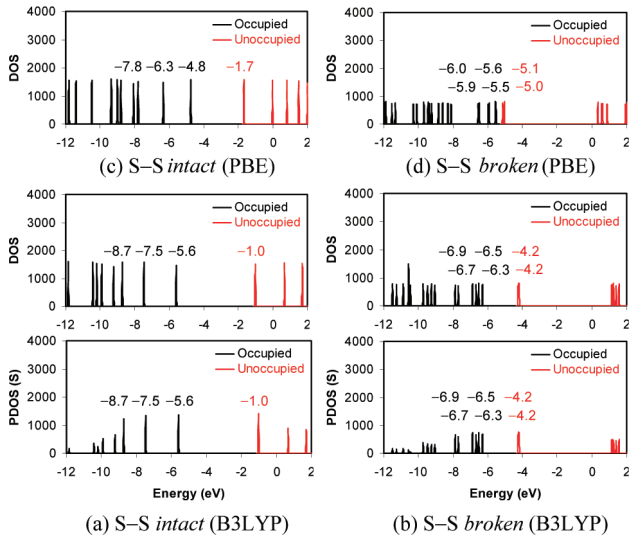

Figure 1. DOS and PDOS onto sulfur atoms of (a,c) cyclic and (b,d) acyclic 1,2-dithiolane.

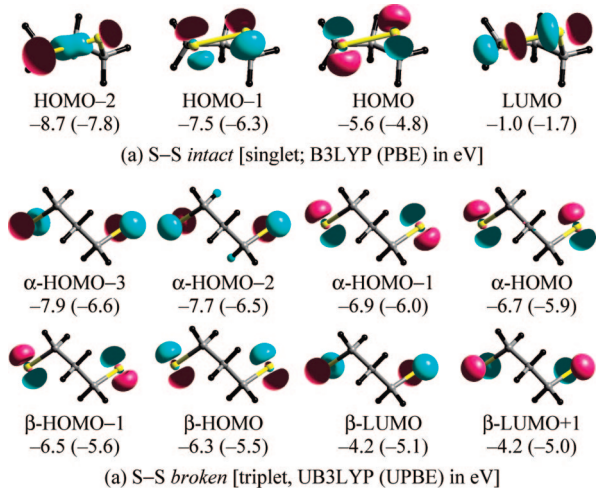

Figure 2. FMOs of (a) cyclic and (b) acyclic 1,2-dithiolane (S, yellow; C, gray; H, black; and different phases of MOs, pink and light blue).

previously.[20] Because the frontier molecular orbitals (FMOs) are essentially of sulfur character (Figures 1 and 2), the difference in HOMO–LUMO gap has a significant effect on the interaction with gold surfaces.

The FMOs of acyclic 1,2-dithiolane are the nonbonding orbitals of two sulfur atoms, which should have energy levels close to each other, with a small HOMO–LUMO gap. Thus, the PBE results seem more reasonable. The main features in the ultraviolet photoemission spectrum (∼4, ∼6, ∼7, and ∼9.5 eV) reported for the molecular state of dimethyl disulfide[70] are also close to the eigenvalues from PBE (4.8, 6.3, 7.8, 8.0, and 8.8 eV). However, it should be noted that the DFT eigenvalues are not rigorously associated with excitation/ionization energies. Thus, the agreement between calculated and predicted gaps (excitation/ionization energies) does not prove the quality of the DFT functionals.

3.2. 1,2-Dithiolane/Au_{28}. The optimized gas-phase structures of cyclic and acyclic 1,2-dithiolane were positioned on Au_{28} clusters in a variety of combinations of different adsorption sites, orientations, and conformations. Each of the two sulfur atoms of 1,2-dithiolane sits on either a bridge or a hollow site of Au(111). The CSSC plane of cyclic 1,2-dithiolane is either tilted

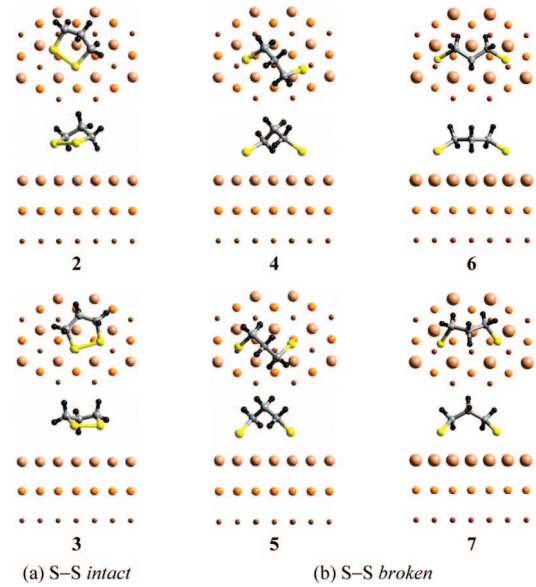

Figure 3. (a) Cyclic and (b) acyclic 1,2-dithiolane on the Au_{28} cluster. The best structure is **4.**

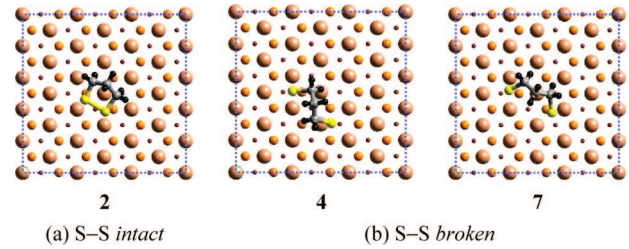

Figure 4. (a) Cyclic and (b) acyclic 1,2-dithiolanes on Au(111) slabs. The best structure is **4**.

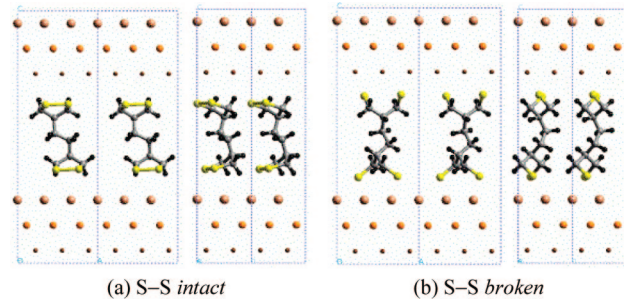

Figure 5. Model junction devices with (a) cyclic and (b) acyclic 1,2-dithiolane anchors on (3 × 2) unit cells of Au(111) electrode surfaces.

toward or perpendicular to the surface. Each torsion angle of the acyclic 1,2-dithiolane is either cis or trans.

The geometry was optimized with B3LYP while the Au_{28} atoms were fixed at their bulk positions. The structures all converged toward several major configurations, **2**−**7** (Figure 3). At the optimum geometry, the binding energy [BE = E(1,2-dithiolane) + E(Au_{28}) − E(1,2-dithiolane/Au_{28})] was evaluated using both B3LYP and PBE. The final properties are reported in Table 1. Without counterpoise correction, the calculated BEs might be subject to a basis set superposition error, but the relative BEs of different conformers of the same species, which are of primary interest in this work, would not be affected significantly by this possibility.

Cyclic 1,2-dithiolane exhibits two primary adsorption structures (**2** and **3**) of which the most stable is **2** [BE = 2.0 (B3LYP) or 11.5 (PBE) kcal/mol], with the 4-CH_2 group pointing away

from the surface. **3** is bound by 1.3 (B3LYP) or 2.2 (PBE) kcal/mol less and has the 4-CH_2 group pointing toward the surface. One sulfur atom sits on a hexagonal close-packed (hcp) hollow site, and the other sits in an asymmetric site because the S—S bond distance (2.15 Å) does not match the distance between the hollow sites of Au(111) (1.7 or 2.9 Å).

Acyclic 1,2-dithiolane exhibits four major adsorption structures (**4**—**7**) of which the most stable is **4**, with a BE of 4.5 (B3LYP) or 19.7 (PBE) kcal/mol with respect to gas-phase cyclic 1,2-dithiolane (51.5 kcal/mol with respect to the gas-phase acyclic structure or 25.8 kcal/mol per Au—S bond). This BE of **4** might be exaggerated because of an edge effect, as one sulfur atom is bound near an edge of the cluster. The PBE binding energies are 11.5 kcal/mol for cyclic 1,2-dithiolane (**2**) and 19.7 kcal/mol for acyclic 1,2-dithiolane (**4**). Thus, dissociative adsorption is preferred.

The discrepancy in BEs between the two functionals of DFT seems to be related to the discrepancy in HOMO–LUMO gap of 1,2-dithiolane [4.6 eV (cyclic) and 2.1 eV (acyclic) when calculated with B3LYP; 3.1 eV (cyclic) and 0.4 eV (acyclic) with PBE]. These FMOs, which are localized at the sulfur anchor group and have good overlap with the Au orbitals, are positioned at energy levels closer to the Au Fermi level with PBE than with B3LYP. Therefore, the interaction of 1,2-dithiolane with Au through the sulfur anchor group should be calculated to be stronger with PBE than with B3LYP.

3.3. 1,2-Dithiolane/Au(111). Adsorption of 1,2-dithiolane was also investigated on an infinite three-layer Au(111) slab using a large periodic unit cell to investigate whether an edge effect is involved in the strong adsorption of **4**. The rectangular ($3\sqrt{3} \times 5$) unit cell with cell parameters of 14.99 × 14.42 × 23.56 (in Å) (Figure 4) allows ~10 Å of free space between 1,2-dithiolanes in adjacent unit cells and ~13 Å of free space between 1,2-dithiolane and the slab above it, leading to a low coverage of 1,2-dithiolane on Au(111). The result should be comparable to the cluster calculations, except for the lack of edge effects. Indeed, we calculated the S—S dissociation energy of a free 1,2-dithiolane molecule as 51.6 kcal/mol (PBE), which is comparable to the value from the molecular calculation (50.9 kcal/mol with PBE).

The calculated BEs of 1,2-dithiolanes on Au(111) slabs are listed in Table 2. We considered two basis sets for Au (DZP and SZP). We also considered the effects of relaxation of the top Au layer, keeping other Au atoms at their experimental bulk positions. Independent of basis set used for Au (DZP or SZP) and independent of whether the top Au layer was allowed to relax, all calculations indicated that acyclic structure **4** is the most stable adsorption configuration, as was found for the cluster calculations on Au_{28}. This conclusion should be reliable because possible edge effects have been eliminated. Allowing the top Au layer to relax leads to the most reliable energies, making acyclic structure **4** more stable than cyclic structure **2** by 8 kcal/mol. (When the top Au layer is not relaxed, the acyclic **4** is more stable by 2 kcal/mol.)

3.4. *I*—*V* Calculations. To determine how the structure of 1,2-dithiolane would affect the *I*—*V* characteristics, we constructed two devices in an electrode—SAM—electrode configuration [Au(111)/dithiolane—CH_2CH_2—dithiolane/Au(111)]. One included the cyclic 1,2-dithiolane (**2**) as the SAM component, and the other contained the acyclic 1,2-dithiolane (**4**) (Figure 5). The DOS, PDOS, and *I*—*V* curves calculated for these model devices are shown in Figures 6 and 7.

Near the Fermi level, the DOS of the isolated SAM of junction molecules (dithiolane—CH_2CH_2—dithiolane) (Figure 6, top) are similar to that of gas-phase 1,2-dithiolane calculated with PBE (Figure 1c,d). Thus, we expect that the MO representations in Figure 2 characterize these levels. The nonbonding orbitals of the sulfur atoms in the acyclic 1,2-dithiolane junction molecule (around −6 eV) form the bonding

TABLE 1: 1,2-Dithiolane/Au_{28} Calculated with B3LYP and PBE[a]

	h(S)[b] (Å)	r(S—Au) (Å)	r(S—S) (Å)	q_{ads}[c] (lel)	BE (kcal/mol)
			S—S *intact*		
2 (singlet)	2.82, 2.89	3.0—3.6	2.154	0.54 (0.61)	2.0 (11.5)
3 (singlet)	2.90, 2.90	3.2—3.6	2.145	0.48 (0.55)	0.7 (9.3)
			S—S *broken*		
4 (singlet)	**2.21, 2.26**	**2.5—3.1**	**4.459**	**0.44 (0.58)**	**4.5 (19.7)**
5 (triplet)	2.10, 2.20	2.5—2.9	4.036	0.41 (0.55)	0.9 (14.6)
6 (triplet)	2.27, 2.27	2.5—3.2	5.351	0.43 (0.57)	1.1 (15.6)
7 (triplet)	2.22, 2.24	2.5—3.3	4.394	0.45 (0.59)	−0.9 (12.4)

[a] Expected best values are in bold. PBE values are in parentheses. [b] h(S) is the height of a sulfur atom from the first layer of Au_{28}. [c] q_{ads} is the Mulliken charge carried by 1,2-dithiolane.

TABLE 2: BEs of 1,2-Dithiolane on a ($3\sqrt{3} \times 5$) Unit Cell of Au(111)[a]

	Au fixed[c]		Au surface optimized[d]	
	DZP[b]	SZP-Au[b]	DZP[b]	SZP-Au[b]
		S—S *intact*		
2 (singlet)	7.5	8.3	8.8	8.9
		S—S *broken*		
4 (singlet)	**9.3**	**10.5**	**16.7**	**17.3**
7 (singlet)	4.4	6.3	8.9	10.4

[a] Calculated with PBE (kcal/mol). Expected best values are in bold. [b] DZP or SZP basis set for Au with Troullier—Martins pseudopotential. DZP basis sets and Hamann-type pseudopotentials for C, H, and S. [c] Only 1,2-dithiolane optimized with Au atoms fixed at bulk positions. [d] First surface layer in contact with 1,2-dithiolane also optimized.

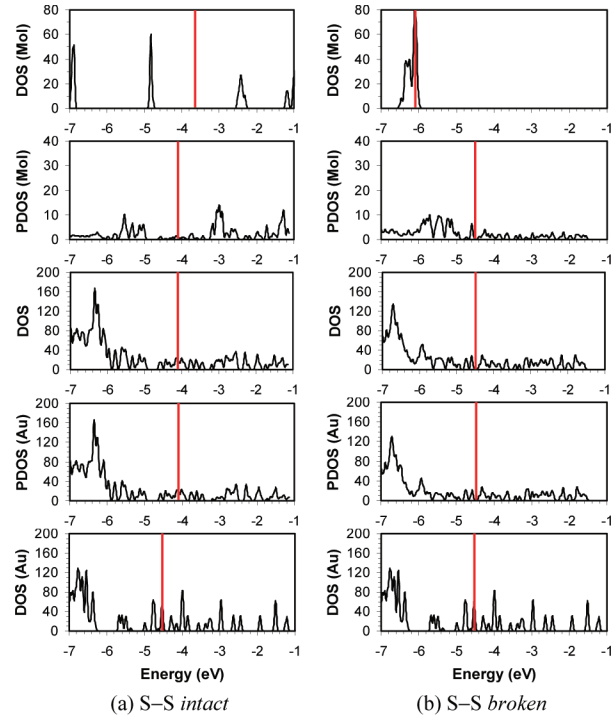

(a) S–S *intact* (b) S–S *broken*

Figure 6. DOS and PDOS of model junction devices of (a) cyclic and (b) acyclic 1,2-dithiolanes. Vertical red lines represent the Fermi levels.

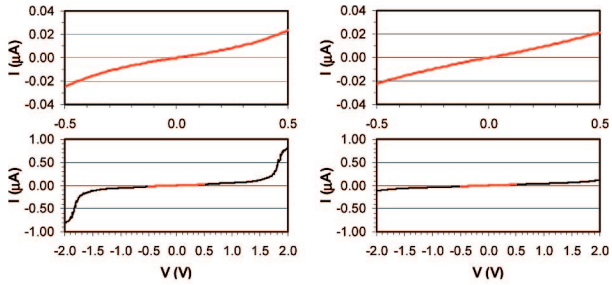

Figure 7. $I-V$ curves of model junction devices of (a) cyclic and (b) acyclic 1,2-dithiolanes, shown for different ranges of bias voltage.

and antibonding orbitals of the disulfide bonds in the cyclic structure with a significant splitting in energy levels (−7, −5, and −2.5 eV).

These FMOs of cyclic and acyclic 1,2-dithiolane junction molecules interact significantly with the Au atomic orbitals, as indicated by the broadening and shifting of the peaks in the PDOS curves of the molecular part (Figure 6, second from the top). However, their contributions to the total DOS near the Fermi level remain very small in both cases. Therefore, we expect only a small amount of current through these molecular junctions for moderate bias voltages.

Indeed, the two junctions show similar insulating characteristics over a moderate range of bias voltages up to ±1.8 V.

The junction with the acyclic 1,2-dithiolane anchor is essentially insulating up to ±2 V (Figure 7b). The current, I, was calculated as 0.37, 3.8, 7.8, 22.1, and 115 nA at 0, ±0.1, ±0.2, ±0.5, and ±2 V, respectively. The conductance G (= dI/dV) is 37 nS at 0 V, with a small bump of 52 nS at ±0.46 V.

The junction with the cyclic 1,2-dithiolane anchor is also insulating up to ±1.8 V (Figure 7a). The current was calculated as 0.31, 3.1, 8.8, and 24.7 nA at 0, ±0.1, ±0.2, and ±0.5 V, respectively. The conductance is 30 nS at 0 V, with a small bump at 84 nS at ±0.54 V.

Because the bias voltage to read molecular junctions typically stays under 1 V, the 1,2-dithiolane anchor would show the same insulating electron transport whether it is in the cyclic or acyclic form in the junction.

At bias voltages higher than 1.8 V, the cyclic 1,2-dithiolane junction shows a large increase in current, reaching a current of 822 nA at ±2 V (Figure 7a). The conductance has a prominent peak of 4.16 μS at ±1.8 V.

Because the Fermi level of the cyclic junction is −4.1 eV, this surge at ±1.8 V is likely due to the molecular levels near −5.0 and −3.2 eV, which correspond to the π- and σ-antibonding disulfide bonds (HOMO and LUMO in Figure 2a). More likely, it is due to the π-antibonding state at −5.0 eV, which has electron clouds protruding perpendicular to the electrode surface, giving them stronger interactions across the junction and leading to better electron transport through the junction.

Injection of a complete electron to or from these molecular levels would weaken the disulfide bond, perhaps inducing its cleavage, but this would require bias voltages of around 2 V, which appears unlikely during the normal operation of typical molecular junctions.

In summary, our DFT calculations show that dissociative adsorption of 1,2-dithiolane (cleaving the disulfide bond) on the Au(111) surface is slightly preferred. However, molecular junctions of cyclic and acyclic 1,2-dithiolanes sandwiched between Au(111) electrodes show the same insulating $I-V$ characteristics at moderate bias voltages (<2 V). Therefore, we expect that the formation and cleavage of disulfide bonds during device operation would not affect the robustness of molecular junctions employing 1,2-dithiolane anchor groups. Of course, at higher bias voltages, there could be other reactions.

Acknowledgment. This work was supported by MARCO-FENA, PIMS (Korea), STAR (KICOS, Korea), and Le STUDIUM (Regional agency for research in Région Centre, France). In addition, the facilities used were supported by ONR-DURIP, ARO-DURIP, and KISTI (Korea).

Supporting Information Available: Basis sets used for Au in the periodic QM calculations (Tables S1 and S2), transmission spectra $T(E)$ and the conductance−voltage ($G-V$) curves of the model junction devices (Figure S1). This material is available free of charge via the Internet at http://pubs.acs.org.

References and Notes

(1) Collier, C. P.; Wong, E. W.; Belohradsky, M.; Raymo, F. M.; Stoddart, J. F.; Kuekes, P. J.; Williams, R. S.; Heath, J. R. *Science* **1999**, *285*, 391–394.
(2) Wong, E. W.; Collier, C. P.; Behloradsky, M.; Raymo, F. M.; Stoddart, J. F.; Heath, J. R. *J. Am. Chem. Soc.* **2000**, *122*, 5831–5840.
(3) Cheng, Q.; Brajter-Toth, A. *Anal. Chem.* **1992**, *64*, 1998–2000.
(4) Tseng, H.-R.; Wu, D.; Fang, N. X.; Zhang, X.; Stoddart, J. F. *ChemPhysChem* **2004**, *5*, 111–116.
(5) Yu, H.; Luo, Y.; Beverly, K.; Stoddart, J. F.; Tseng, H.-R.; Heath, J. R. *Angew. Chem., Int. Ed.* **2003**, *42*, 5706–5711.
(6) Cooke, G.; Duclairoir, F. M. A.; Rotello, V. M.; Stoddart, J. F. *Tetrahed. Lett.* **2000**, *41*, 8163–8166.
(7) Azehara, H.; Mizutani, W.; Suzuki, Y.; Ishida, T.; Nagawa, Y.; Tokumoto, H.; Hiratani, K. *Langmuir* **2003**, *19*, 2115–2123.
(8) Herranz, M. A.; Yu, L.; Martin, N.; Echegoyen, L. *J. Org. Chem.* **2003**, *68*, 8379–8385.
(9) Herranz, M. A.; Colonna, B.; Echegoyen, L. *Proc. Natl. Acad. Sci.* **2002**, *99*, 5040–5047.
(10) Wang, Y.; Kaifer, A. E. *J. Phys. Chem. B* **1998**, *102*, 9922–9927.
(11) Blonder, R.; Willner, I.; Buckmann, A. F. *J. Am. Chem. Soc.* **1998**, *120*, 9335–9341.
(12) Carofiglio, T.; Fornasier, R.; Jicsinszky, L.; Tonellato, U.; Turco, C. *Tetrahedron Lett.* **2001**, *42*, 5241–5244.
(13) Madoz, J.; Kuznetzov, B. A.; Medrano, F. J.; Garcia, J. L.; Fernandez, V. M. *J. Am. Chem. Soc.* **1997**, *119*, 1043–1051.
(14) Miura, Y.; Kimura, S.; Imanishi, Y.; Umemura, J. *Langmuir* **1998**, *14*, 6935–6940.
(15) Heath, J. R.; Ratner, M. A. *Phys. Today* **2003**, *56*, 43–49.
(16) Green, J. E.; Choi, J. W.; Boukai, A.; Bunimovich, Y.; Johnston-Halperin, E.; Delonno, E.; Luo, Y.; Sheriff, B. A.; Xu, K.; Shin, Y. S.; Tseng, H.-R.; Stoddart, J. F.; Heath, J. R. *Nature* **2007**, *445*, 414–417.
(17) Balzani, V.; Credi, A.; Mattersteig, G.; Matthews, O. A.; Raymo, F. M.; Stoddart, J. F.; Venturi, M.; White, A. J. P.; Williams, D. J. *J. Org. Chem.* **2000**, *65*, 1924–1936.
(18) Tseng, H.-R.; Vignon, S. A.; Stoddart, J. F. *Angew. Chem., Int. Ed.* **2003**, *42*, 1491–1495.
(19) Jang, Y. H.; Goddard, W. A., III *J. Phys. Chem. B* **2006**, *110*, 7660–7665.
(20) Jang, Y. H.; Hwang, S.; Kim, Y.-H.; Jang, S. S.; Goddard, W. A., III *J. Am. Chem. Soc.* **2004**, *126*, 12636–12645.
(21) Deng, W.-Q.; Muller, R. P.; Goddard, W. A., III *J. Am. Chem. Soc.* **2004**, *126*, 13562–13563.
(22) Kim, Y.-H.; Jang, S. S.; Jang, Y. H.; Goddard, W. A., III *Phys. Rev. Lett.* **2005**, *94*, 156801.
(23) Jang, Y. H.; Jang, S. S.; Goddard, W. A., III *J. Am. Chem. Soc.* **2005**, *127*, 4959–4964.
(24) Jang, S. S.; Jang, Y. H.; Kim, Y.-H.; Goddard, W. A., III; Flood, A. H.; Laursen, B. W.; Tseng, H.-R.; Stoddart, J. F.; Jeppesen, J. O.; Choi, J. W.; Steuerman, D. W.; DeIonno, E.; Heath, J. R. *J. Am. Chem. Soc.* **2005**, *127*, 1563–1575.
(25) Jang, S. S.; Jang, Y. H.; Kim, Y.-H.; Goddard, W. A., III; Choi, J. W.; Heath, J. R.; Laursen, B. W.; Flood, A. H.; Stoddart, J. F.; Norgaard, K.; Bjornholm, T. *J. Am. Chem. Soc.* **2005**, *127*, 14804–14816.
(26) Kim, Y.-H.; Goddard, W. A., III *J. Phys. Chem. C* **2007**, *111*, 4831–4837.
(27) Flood, A. H.; Peters, A. J.; Vignon, S. A.; Steuerman, D. W.; Tseng, H.-R.; Kang, S.; Heath, J. R.; Stoddart, J. F. *Chem. Eur. J.* **2004**, *10*, 6558–6564.

(28) Kang, S.; Vignon, S. A.; Tseng, H.-R.; Stoddart, J. F. *Chem. Eur. J.* **2004**, *10*, 2555–2564.
(29) Braunschweig, A. B.; Dichtel, W. R.; Miljanic, O. S.; Olson, M. A.; Spruell, J. M.; Khan, S. I.; Heath, J. R.; Stoddart, J. F. *Chem. Asian J.* **2007**, *2*, 634–647.
(30) Choi, J. W.; Flood, A. H.; Steuerman, D. W.; Nygaard, S.; Braunschweig, A. B.; Moonen, N. N. P.; Laursen, B. W.; Luo, Y.; DeIonno, E.; Peters, A. J.; Jeppesen, J. O.; Xu, K.; Stoddart, J. F.; Heath, J. R. *Chem. Eur. J.* **2006**, 261–279.
(31) DeIonno, E.; Tseng, H.-R.; Harvey, D. D.; Stoddart, J. F.; Heath, J. R. *J. Phys. Chem. B* **2006**, *110*, 7609–7612.
(32) Wilhelm, M.; Berssen, E.; Koch, R.; Strasdeit, H. *Monatsh. Chem.* **2002**, *133*, 1097–1108.
(33) Howie, J. K.; Houts, J. J.; Sawyer, D. T. *J. Am. Chem. Soc.* **1977**, *99*, 6223–6326.
(34) Antonello, S.; Holm, A. H.; Instuli, E.; Maran, F. *J. Am. Chem. Soc.* **2007**, *129*, 9836–9837.
(35) Dong, Y.; Abaci, S.; Shannon, C.; Bozack, M. J. *Langmuir* **2003**, *19*, 8922–8926.
(36) Fujihara, H.; Nakai, H.; Yoshihara, M.; Maeshima, T. *Chem. Commun.* **1999**, 737–738.
(37) Maksymovych, P.; Yates; J, T., Jr. *J. Am. Chem. Soc.* **2006**, *128*, 10642–10643.
(38) Nuzzo, R. G.; Zegarski, B. R.; Dubois, L. H. *J. Am. Chem. Soc.* **1987**, *109*, 733–740.
(39) Fenter, P.; Eberhardt, A.; Eisenberger, P. *Science* **1994**, *266*, 1216–1218.
(40) Gerdy, J. J.; Goddard, W. A., III *J. Am. Chem. Soc.* **1996**, *118*, 3233–3236.
(41) Zhou, J.-G.; Williams, Q. L.; Hagelberg, F. *Phys. Rev. B* **2007**, *76*, 075408.
(42) Vericat, C.; Vela, M. E.; Salvarezza, R. C. *Phys. Chem. Chem. Phys.* **2005**, *7*, 3258–3268.
(43) Roper, M. G.; Jones, R. G. *Phys. Chem. Chem. Phys.* **2008**, *10*, 1336–1346.
(44) De Renzi, V.; Rousseau, R.; Marchetto, D.; Biagi, R.; Scandolo, S.; del Pennino, U. *Phys. Rev. Lett.* **2005**, *95*, 046804.
(45) Yourdshahyan, Y.; Rappe, A. M. *J. Chem. Phys.* **2002**, *117*, 825–833.
(46) *Jaguar 5.5*; Schrodinger Inc.: Portland, OR, 2003.
(47) Jacob, T.; Muller, R. P.; Goddard, W. A., III *J. Phys. Chem. B* **2003**, *107*, 9465–9476.
(48) Maeland, A.; Flanagan, T. B. *Can. J. Phys.* **1964**, *42*, 2364–2366.
(49) Slater, J. C. *Quantum Theory of Molecules and Solids. Vol. 4. The Self-Consistent Field for Molecules and Solids*; McGraw-Hill: New York, 1974.
(50) Becke, A. D. *Phys. Rev. A* **1988**, *38*, 3098–3100.
(51) Vosko, S. H.; Wilk, L.; Nusair, M. *Can. J. Phys.* **1980**, *58*, 1200–1211.
(52) Lee, C.; Yang, W.; Parr, R. G. *Phys. Rev. B* **1988**, *37*, 785–789.
(53) Miehlich, B.; Savin, A.; Stoll, H.; Preuss, H. *Chem. Phys. Lett.* **1989**, *157*, 200–206.
(54) Perdew, J. P.; Burke, K.; Ernzerhof, M. *Phys. Rev. Lett.* **1996**, *77*, 3865–3868.
(55) Perdew, J. P.; Burke, K.; Ernzerhof, M. *Phys. Rev. Lett.* **1997**, *78*, 1396–1396.
(56) Hay, P. J.; Wadt, W. R. *J. Chem. Phys.* **1985**, *82*, 299–310.
(57) Melius, C. F.; Olafson, B. D.; Goddard, W. A., III *Chem. Phys. Lett.* **1974**, *28*, 457–462.
(58) Schultz, P. A.; Muller, R. P. *SeqQuest Electronic Structure Code*; Sandia National Laboratories: Albuquerque, NM; available at http://dft.sandia.gov/Quest.
(59) Williams, A. R.; Feibelman, P. J.; Lang, N. D. *Phys. Rev. B* **1982**, *26*, 5433–5444.
(60) Feibelman, P. J. *Phys. Rev. B* **1987**, *35*, 2626–2646.
(61) Hamann, D. R. *Phys. Rev. B* **1989**, *40*, 2980–2987.
(62) Redondo, A.; Goddard, W. A., III; McGill, T. C. *Phys. Rev. B* **1977**, *15*, 5038–5048.
(63) Troullier, N.; Martins, J. L. *Phys. Rev. B* **1991**, *43*, 1993–2006.
(64) Fuchs, M.; Scheffler, M. *Comput. Phys. Commun.* **1999**, *119*, 67–98.
(65) Feibelman, P. J. *Phys. Rev. B* **1988**, *38*, 1849–1855.
(66) Kim, Y.-H.; Jang, S. S.; Goddard, W. A., III *J. Chem. Phys.* **2005**, *122*, 244703.
(67) Kim, Y.-H.; Tahir-Kheli, J.; Schultz, P. A.; Goddard, W. A., III *Phys. Rev. B* **2006**, *73*, 235419.
(68) Datta, S. *Quantum Transport: Atom to Transistor*; Cambridge University Press: Cambridge, UK, 2005.
(69) Stroud, R. M.; Carlisle, C. H. *Acta Crystallogr. B* **1972**, *28*, 304–307.
(70) De Renzi, V. *Surf. Sci.* **2007**, *601*, 2592–2596.

JP800201Z